December 2017

Exterior Giant Planet Effects on Terrestrial Architecture

Anna Corinne Childs
University of Nevada, Las Vegas, childs.annacorinne@gmail.com

EXTERIOR GIANT PLANET EFFECTS ON TERRESTRIAL ARCHITECTURE

by

Anna Corinne Childs

Bachelor of Science – Mathematics
University of Nevada, Las Vegas
2014

A thesis submitted in partial fulfillment
of the requirements for the

Master of Science – Physics

Department of Physics and Astronomy
College of Sciences
The Graduate College

University of Nevada, Las Vegas
December 2017

UNLV | GRADUATE COLLEGE

Thesis Approval

The Graduate College
The University of Nevada, Las Vegas

November 14, 2017

This thesis prepared by

Anna Corinne Childs

entitled

Exterior Giant Planet Effects on Terrestrial Architecture

is approved in partial fulfillment of the requirements for the degree of

Master of Science - Physics
Department of Physics and Astronomy

Jason Steffen, Ph.D.
Examination Committee Chair

Rebecca Martin, Ph.D.
Examination Committee Member

Zhaohuan Zhu, Ph.D.
Examination Committee Member

Arya Udry, Ph.D.
Graduate College Faculty Representative

Kathryn Hausbeck Korgan, Ph.D.
Graduate College Interim Dean

Abstract

Terrestrial planet formation is a chaotic and violent process which is not fully understood. Prior to *Kepler*, Solar System observations were the basis for planet formation models. However, *Kepler* observations have shown that exoplanet systems are very different from our solar system, thus requiring a more complete planet formation model. With advancements in computational ability, N-body integrators, and collision models, we can explore planet formation by experimenting with simulations in different parameter space. Our Solar System has shown us that exterior giant planets can play a vital role in the shaping of the final terrestrial planet system. Our recent N-body simulations have explored the relationship between exterior giant planets of varying mass and size, and final terrestrial planet architecture. Here we present the results from our simulations. Understanding the relationship between the presence of giant planets and terrestrial system structure will help us interpret observation, and aid in the formulation of a general, terrestrial planet formation model.

Acknowledgements

I would first like to thank my thesis advisor, Dr. Jason Steffen. He took me on as a graduate student when I had absolutely no background in astronomy. If it weren't for his continuous support, guidance and patience, I wouldn't be where I'm at in the field today.

I would like to acknowledge Dr. Elisa Quintana and Dr. Thomas Barclay for mentoring me throughout the course of this research project and whose contributions to my education have been absolutely vital to this thesis.

I would also like to thank my committee members who put in their time and expertise to help validate this thesis: Dr. Jason Steffen, Dr. Rebecca Martin, Dr. Zhaohuan Zhu, and Dr. Arya Udry.

Finally, I must express my very profound gratitude to all my family and friends who continue to support me in every facet of my journey in education. Thank you.

Dedication

Dedicated to my mother: the best study partner a graduate student could have.

Table of Contents

List of Tables

List of Figures

List of Symbols

Q	*Toomre Q* parameter
c_s	sound speed
Ω	Keplerian angular velocity
G	Acceleration of gravity
$M_\star$	Star mass
a	Semi-major axis
Σ	Surface density distribution
v_{esc}	Escape velocity
σ	Relative velocity of two objects at infinity
$Q^\star_{RD}$	Catastrophic disruption criteria
$V^\star$	Critical impact velocity

μ	Reduce mass
M_{tot}	Total mass
M_p	Projectile mass
M_{targ}	Target mass
$Q'^{\star}_{RD}$	Catastrophic disruption threshold
Q_r	Specific impact energy
θ	Impact angle
ξ	Accretion efficiency
M_{lr}	Mass of largest remnant
r	Radius
$R_{\oplus}$	Earth radius
$M_{\oplus}$	Earth mass
$\tau_{evolution}$	Evolution timescale

List of Abbreviations

NASA	National Aeronautics and Space Administration
AU	Astronomical unit
Myr	Million years
KOI	Kepler Object of Interest
TESS	Transiting Exoplanet Survey Satellite
JWST	James Webb Space Telescope
RV	Radial velocity

Chapter 1

Introduction

Planet formation is not a fully understood process. The formation of our Solar System still poses many questions and exoplanet observations have shown us that planetary systems can be vastly different from the Solar System. The observed diversity of exoplanet systems has motivated studies of planet formation. The different classes of planets can be formed through very different processes, and there is still much to learn about the formation process. This thesis is particularly interested with the formation of terrestrial planets and the effects giant planets have on final terrestrial planet architecture.

Terrestrial planet formation

Terrestrial planet formation is typically broken into three stages: the early-stage, mid-stage, and late-stage. The early-stage of planet formation focuses on the growth of dust particles in a gas disc to planetesimals, the mid-stage studies the formation process of planetesimals to embryos, and the late-stage deals with the growth of embryos into planets. The physics differ in each stage and of these three stages, the late-stage is the most widely understood. At this stage in planet formation you have solid bodies of varied masses interacting with one another through purely gravitational mechanisms. This becomes an N-body problem best handled with an N-body integrator. *Mercury* is a very popular N-body integrator used to study planet formation (Chambers (2001)). Previously, N-body simulations assumed relatively trivial collisions. Collision outcomes were limited to either *completely elastic* or *completely inelastic* collisions. However, we know that collision outcomes are much more dynamic than this. An accurate collision model is imperative to fully understand terrestrial planet formation. The internal structure and moon system of a terrestrial planet is very dependent upon its collision history. It may also have implications for the overall architecture of the system.

(Leinhardt & Stewart (2012)) developed a dynamic description of more realistic collisions. Their collision model allows for fragmentation, hit-and-run collision, perfect accretion, and cratering. In 2013 Chambers implemented this fragmentation model into *Mercury* (Chambers (2013)). With this updated collision model implemented into *Mercury*, we are able to probe planet formation in greater detail.

1.1 The role of Jupiter & Saturn

When studying planet formation, the Solar System is typically the base model for studies as it offers the most detailed observations and information of any planetary system to date. Observation from *Kepler* however, has showed us that the Solar System is very different from the majority of known exoplanet systems. Still, the studies done with the Solar System as a base model, have provided us with valuable insight into planet formation.

A study by (Horner & Jones (2008)) found from N-body simulations, that Jupiter and Saturn played a vital role in shaping the habitability of Earth. They found that without the influence of Saturn and Jupiter, the Earth would have been susceptible to a punishable rate of high-energy impacts that would have prevented the development of life. Other studies showed that the presence of giant planets also shapes the overall structure of the system (Quintana et al. (2016)). Simulations have shown that systems with and without giant planets, form terrestrial systems of different multiplicities, and terrestrial planets of different sizes with different orbits. These studies motivated us to explore in further detail the extent to which giant planets interact with the protoplanetary disk and shape the architecture of the terrestrial planet system.

1.2 Giant planets of varying mass

Motivated by other studies that show how giant planets can potentially alter the formation of terrestrial planets in a system, we have conducted a series of N-body integrations using the updated collision model from (Leinhardt & Stewart (2012)), to study how the mass of exterior giant planets shapes the terrestrial planet structure of a system. We considered five systems of similar protoplanetary disks while varying the masses at Saturn's & Jupiter's current orbit. Maintaining a 3:1 mass ratio of the planets at Jupiter's & Saturn's current orbits, we varied the masses and integrated for at least five million years to determine the effects of these giant planets on the formation of the terrestrial planets in the system. This paper presents the setup, results, conclusions, and implications from those simulations.

Chapter 2

Terrestrial planet formation

2.1 Stages of terrestrial planet formation

In this section, we overview the current leading theory on late-stage planet formation. Terrestrial planet formation has been broken down into three stages. The first stage (early-stage) is the dust to planetesimal formation, the second stage (mid-stage) is the planetesimals to embryos stage, and the last stage (late-stage) is the growth of embryos to form planets. The physics between the different stages in terrestrial planet formation differ drastically and thus require different approaches to understand the key processes involved. The work discussed here deals specifically with the late-stage of terrestrial planet formation. The beginning of late-stage planet formation is defined to be when bodies are formed and are large enough such that each bodies orbital evolution is dominated by gravitational interactions with other bodies in the disk. Through a series of dynamic, gravitationally dominated interactions with other bodies in the protoplanetary disk, bodies grow until they become planets.

2.1.1 Dust to planetesimals

Of the three stages of planet formation, the growth from dust to planetesimals is the least understood. This lack of understanding is attributed to the complexities that arrise when considering the gas dynamics involved in this phase. At this time, a gas disk remains, the dust particles are small, and the gas-gas particle, gas-dust particle, and dust-dust particle interactions are dynamic (Rafikov (2003)).

A number of mechanisms have been proposed to account for the interactions that would grow dust particles to planetesimals. These proposed mechanisms include: particle sticking, gravitation instability, turbulent concentration, and streaming instability. These planetesimals can form at different regions where different components may be forming at different times, thus leading to different planetesimal composition.

The stability of the gas disk is governed by the *Toomre Q* parameter. After the *Toomre Q* parameter is $Q \approx 1$, gravitational instabilities begin to set in and dust clumping begins. The *Toomre Q* parameter is defined as,

$$Q \equiv \frac{c_s \Omega}{\pi G \Sigma}, \tag{2.1}$$

for sound speed (c_s), Keplerian angular velocity ($\Omega = \sqrt{GM_\star/a^3}$), and the surface density distribution (Σ). As this criteria is met, the dust particles begin to grow. The dust particles first "stick" together through chemical bonds and van der Walls forces, and then are vertically settled into thin sublayers. One of the issues with rapid planetesimal formation is referred to as the *meter-size barrier problem*. This refers to the issue of planetesimals forming too rapidly in a gas disk. If the planetesimal becomes any larger than one meter in the gas disk before a significant amount of the gas has dissipated, the planetesimal will be swept into the star via gas drag. There are regions in a gas disk where this issue may be avoided however. Between turbulent eddies in the gas disk, there may exist stagnant regions where solids may grow beyond one meter through a process referred to as *turbulent concentration*. In these stagnant regions, high solid/gas ratios (≈ 100) may form, thus allowing larger solids to form without the threat of being swept away by gas drag.

If meter-sized planetesimals form via particle sticking before the gas dissipates, another proposed mechanism of planetesimal growth is referred to as *streaming instability*. This occurs when multiple inward drifting planetesimals collide, expereince a reduced headwind, become gravitationally unstable and are then able to grow into planetesimals hundreds of km in size (Righter & O'Brien (2011)).

2.1.2 Embryo formation

After the formation of a planetesimal disk, embryo's form through planetesimal-planetesimal interactions. Planetesimals may now experience *runaway growth* where they gravitationally interact with each other and accrete one another once their relative velocities are comparable to their escape velocities. These growing bodies are now referred to as embryos and dynamically excite the remaining planetesimals in the disk via gravitational interactions. These dynamic excitations result in an increase of the planetesimal velocities and their spatial distributions and the embryos experience what is referred to as *oligarchic growth*. *Oligarchic growth* is dominated by the embryo due to its ability to gravitationally focus planetesimals and other embryos (Righter & O'Brien (2011)). Gravitational focusing is when a bodies collisional cross-section exceeds it's geometric cross-section due to its gravitational influence. The cross-section enhancement term is given by:

$$(1 + \frac{v_{esc}^2}{\sigma^2}), \tag{2.2}$$

where v_{esc} is the projectiles escape velocity and σ is the relative velocity of the two objects at infinity. The result of this *oligarchic growth* is the transition from planetesimals to embryos.

Time scales are very important in the embryo growth and formation process. Not only does it determine which accretion processes will dominate, but it also determines how much gas the embryo will accrete. For example, if the embryo is massive enough and formed before the gas entirely dissipates, the embryo will accrete the gas. Should this formation happen early enough, it may result in a gas giant. Conversely, should embryos form after the gas dissipates, a terrestrial planet may be formed. The research discussed here deals with the latter case.

2.1.3 Embryo to planet transition

The final assembly of terrestrial planets is characterized by high-velocity embryo-embryo collisions. At this point, the embryos have cleared majority of the planetesimal disk and thus dynamical friction can no longer damp the inclination and eccentricity of the embryos. Consequently, the remaining bodies in the disk interact through purely gravitational interactions with high specific energy impacts. N-body integrations are used to study the types of collisions resulting from these gravitational impacts and thus, the formation from embryo to planet at this stage. These high energy embryo-embryo impacts are referred to as *giant impacts*. These impacts influence the growth, composition and habitability of the terrestrial planets that they form, thus having the final say on the terrestrial planet architecture of the system (Quintana et al. (2016)).

Chapter 3

Physics and dynamical outcomes of collisions

3.1 Previous Collision Models

Terrestrial planet formation is a violent process, characterized by the frequency and magnitudes of high energy impacts between solid bodies in the disk. It is largely a planets collision history that is responsible for the final structure of the planet (Quintana et al. (2016)). When studying this collision history, N-body integrators are used to track the chaotic process of planetesimal and embryo collisions. Because the disk is cleared of gas and most of the planetesimals at this stage, there is no dynamical damping of the bodies. This lack of dynamic damping allows the bodies to reach high relative velocities which results in catastrophic collisions.

In previous N-body simulations, collision outcomes were extremely limited. The codes allowed for only two outcomes. Either a *perfect merger*, which is the absolute accretion and conservation of mass every time two bodies come in contact, or a completely *elastic* collision, where there is no exchange or loss of mass for both of the bodies involved in the collision. Of course, these are not accurate collision models and it posed a major limitation for understanding planet formation. As a result, there have been extensive studies on the physics and outcomes of collisions by Leinhardt & Stewart (2012).

Another barrier for achieving high precision N-body simulations with respect to collisions, is computational ability. An accurate collision model must account for collisions which do not result in either perfect accretion or an elastic collision. In implementing this model into a simulator, the machine must be able to track fragments that result from a dynamic collision, and those fragments collisions with the other planetesimals, embryos and fragments in the system. Tracking fragments can become very computationally expensive, and up until relatively recently, such computational ability was not readily available. However, with the technological advancements we've seen in just the last decade, and more comprehensive collision studies, we are able to implement more accurate collision models into N-body integrators and track the resulting bodies accordingly. Although computational ability has improved significantly, it is important to set a minimum fragment mass so the number of bodies in the system does not tend to infinity. A higher minimum mass will yield a lower potential number of bodies, and thus computation time. It is important to set a minimum fragment mass that will allow for a reasonable computation time without compromising the resolution of the collision outcome.

3.2 Curent collision models

Detailed studies of the physics and results of dynamic collisions have only been conducted relatively recently. Here we discuss what has been done, and how these studies have been implemented into numerical codes. Leinhardt & Stewart (2012) derived an analytic description of the dynamical outcome for collisions of solid bodies in a gas-less disk. Their description is characterized by the *catastrophic disruption critera*, $Q^{\star}_{RD}$, which is the specific energy required to gravitationally disperse half the total mass, and the impact conditions. The catastrophic disruption criteria is given by,

$$Q^{*}_{RD} = 0.5\mu V^{*2}/M_{tot}, \tag{3.1}$$

where V^* is critical impact velocity required to disperse half of the total mass in a collision, μ is the reduced mass $M_p M_{targ}/M_{tot}$ for a projectile mass M_p and a target mass M_{targ}, and the total mass is $M_{tot} = M_p + M_{targ}$. This equation describes a set of curves that are functions of size, impact velocity, and material parameters such as density and composition.

Impact conditions depend on the following parameters: target size, projectile size, impact parameter, impact velocity, and the composition and thus strength of the colliding bodies. By evaluating these criteria, the collisions are separated into different regimes or different collision outcomes. The different regimes considered here are: cratering, merging, catastrophic disruption, super-catastrophic disruption, and hit-and-run events. Equations and scaling laws are used to describe each regime and the transitions between regimes. These equations and scaling laws are functions of mass ration, impact angle, and impact velocity. Each regime and its relevant physics will be discussed in the following subsections.

3.2.1 Collision outcomes

Leinhardt & Stewart (2012) define the disruption regime as the group of collisions in which the energy of the collision results in mass loss between $\sim 10\%$ and $\sim 90\%$ of the total mass. Collisions of this type result in the largest remnant having a linear dependence on the specific impact energy. The emperical catastrophic disruption threshold, Q'^{*}_{RD}, is determined by a line of best fit to the plot of the mass of the largest remnant post-collision, and the specific impact energy for different impact scenarios from numerical results from Leinhardt & Stewart (2012). The specific impact energy, Q_R, is the ratio of the kinetic energies of the projectile to the target mass. The impact scenarios are grouped based on fixed mass ratios and impact angles. The impact angle, θ, is defined at the time of first contact as the angle between the line connecting the centers of the two bodies and the normal to the projectile velocity vector (Leinhardt & Stewart (2012)).

The super-catastrophic disruption regime is defined to be when $Q_R/Q'^{*}_{RD} \geq 1.8$. In this regime, the mass of the largest remnant follows a power law distribution with Q_R, rather than the linear dependence as found in the catastrophic disruption regime. Simulation results from Leinhardt & Stewart (2012) found that the dynamical properties of the smaller fragments in super-catastrophic collisions are similar to the catastrophic disruption regime.

A hit-and-run collisions occurs when the collision happens at such an oblique angle, the two bodies separate. The target is left mainly intact and the outcome of the projectile depends on the specifics of the impact. The projectile may be largely unaffected by the collision, or it may suffer large deformation and damage. This collision regime has been parameterized by (Asphaug (2009)). It considers the accretion efficiency given by,

$$\xi = \frac{M_{lr} - M_{targ}}{M_p}, \tag{3.2}$$

where M_{lr} is the mass of the largest post-collision remnant. A perfect hit-and-run collision happens when $M_{lr} = M_{targ}$, and $\xi = 0$. A perfect accretion occurs when $M_{lr} = M_{tot}$, and $\xi = 1$, and an errosive collision is a collision which results in $M_{lr} < M_{targ}$, and $\xi < 0$.

Cratering is an erosive collision and merging is an accretion process. These two scenarios occur at the threshhold of the catastrophic disruption regime. At specific energies lower than necesarry for catastrophic disruption, the resulting collision will either be cratering or merging. Cratering is partial erosion of the target body, and merging is partial accretion of the projectile onto the target body (Leinhardt & Stewart (2012)).

3.3 Current collision models in numerical code

Chambers (2001) released his N-body integrator *Mercury* in 2001. It tracked close encounters, grazing events, ejections and collisions between objects. The collision resulted in either perfect accretion, or a completely elastic collision. In 2013, Chambers implemented a fragmentation model into *Mercury* to track more realistic collision outcomes Chambers (2013). Adopting the models from Leinhardt & Stewart (2012), Chambers developed a code that allowed collisions to produce fragments and allowed those fragments to interact with other bodies in the system.

Quintana et al. (2016) were among the first to use Chambers' fragmentation model. They conducted a series of simulations with *Mercury* to test the fragmentation model by using the same initial conditions and running the simulations with and without the fragmentation code in *Mercury*. Quintana et al. (2016) found that with fragmentation on, the number of bodies in the system decreased much quicker than the simulations without fragmentation, as seen in Figure 1. All though the systems both begin to flatten out around 300 myr, the evolution of the systems is much different. This highlights the importance of a fragmentation model when studying terrestrial planet formation with N-body simulations. As discussed before, terrestrial planet formation is characterized by impacts in the late-stage formation process. The simulations performed by Quintana et al. (2016) showed the importance of incorporating a more realistic collision model into N-body studies.

Chapter 4

N-body simulations

4.1 Set-up

Our initial disk follows a mass distribution of 26 embryos (Mars-sized, $r = 0.56R_{\oplus}$; $m = 0.093M_{\oplus}$), and 260 planetesimals (Moon-sized, $r = 0.26R_{\oplus}$; $m = 0.0093M_{\oplus}$) giving the disk a mass of $4.85M_{\oplus}$. The masses are distributed between 0.35 AU and 4 AU from a solar-type star. All masses have a uniform density of 3 g/cm^3. The surface density distribution of the planetesimals and embryos follows $\Sigma = r^{-3/2}$ as is the predicted surface density distribution of Solar Nebula models (Weidenschilling (1977)). There is no gas in the disk, allowing for purely gravitational collisions. The orbits of all the bodies are nearly coplanar and circular. The eccentricities and inclinations for each body were given a random Rayleigh distribution where $e < 0.01$ and $i < 1°$ as seen in Figure 4.1 as a function of semi-major axis. The argument of periastron, mean anomaly, and longitude of ascending node, were chosen at random. Exterior planets of varying mass are placed at Saturn's and Jupiter's orbit, 5.2 AU and 9.6 AU respectively, with their present orbital elements. Five different systems were used for our simulations. We considered exterior massive planets with 3:1 mass ratios. The masses are given by Table 4.1. 150 realizations were conducted for each system. A slight change of one planetesimal's longitude of ascending node was made for each realization.

Previous work by Quintana et al. (2016) showed that five myr was sufficient time to determine the mass loss trends of a system with respect to mass distribution. Using the same disk the two most extreme cases were considered, a system with Jupiter & Saturn, and

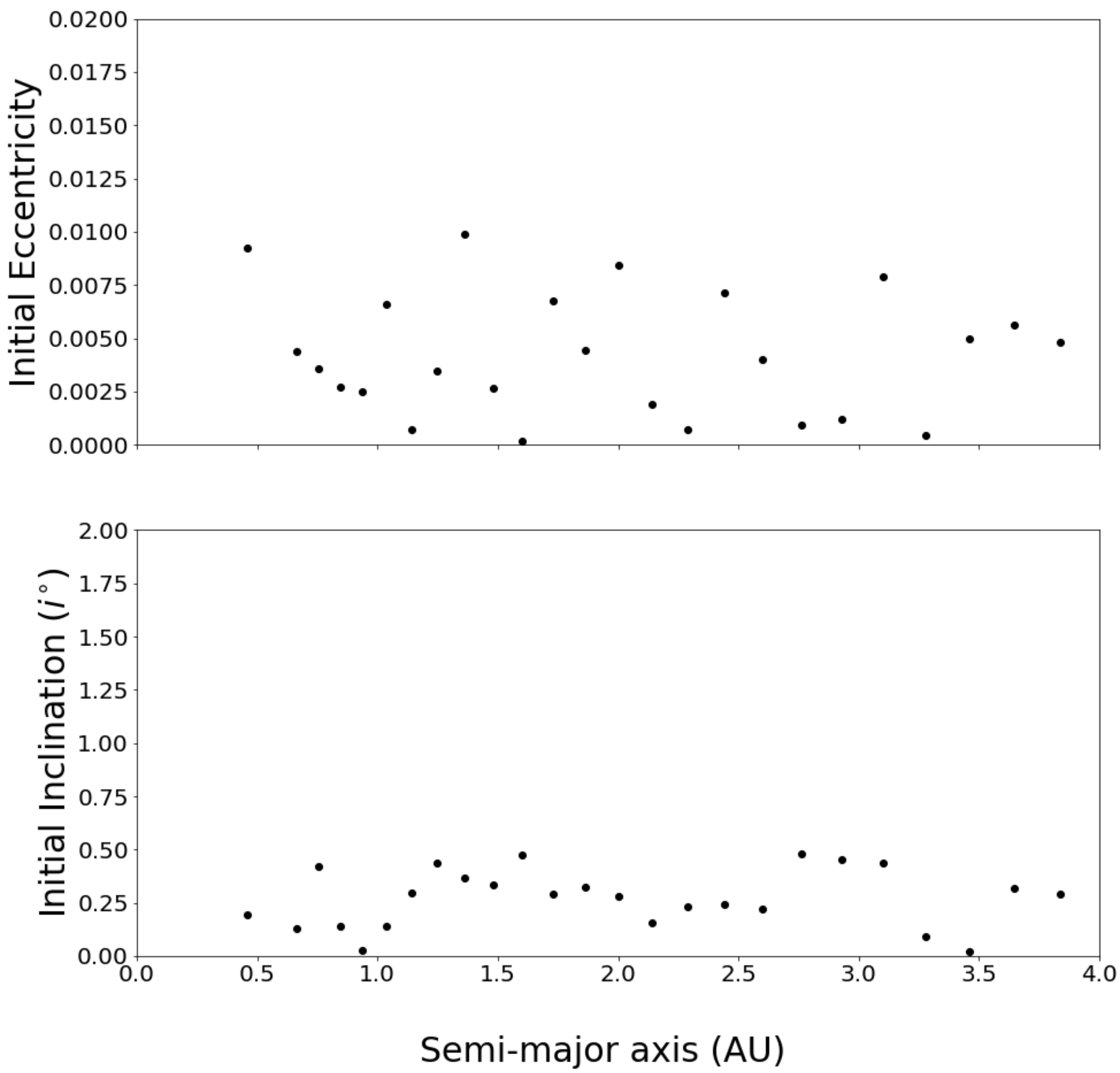

Figure 4.1: Initial eccentricities and inclinations versus semi-major axis for the 26 embryos used in each realization. All the other orbital elements for the embryos are choosen at random. The embryos begin on nearly circular and coplanar orbirts.

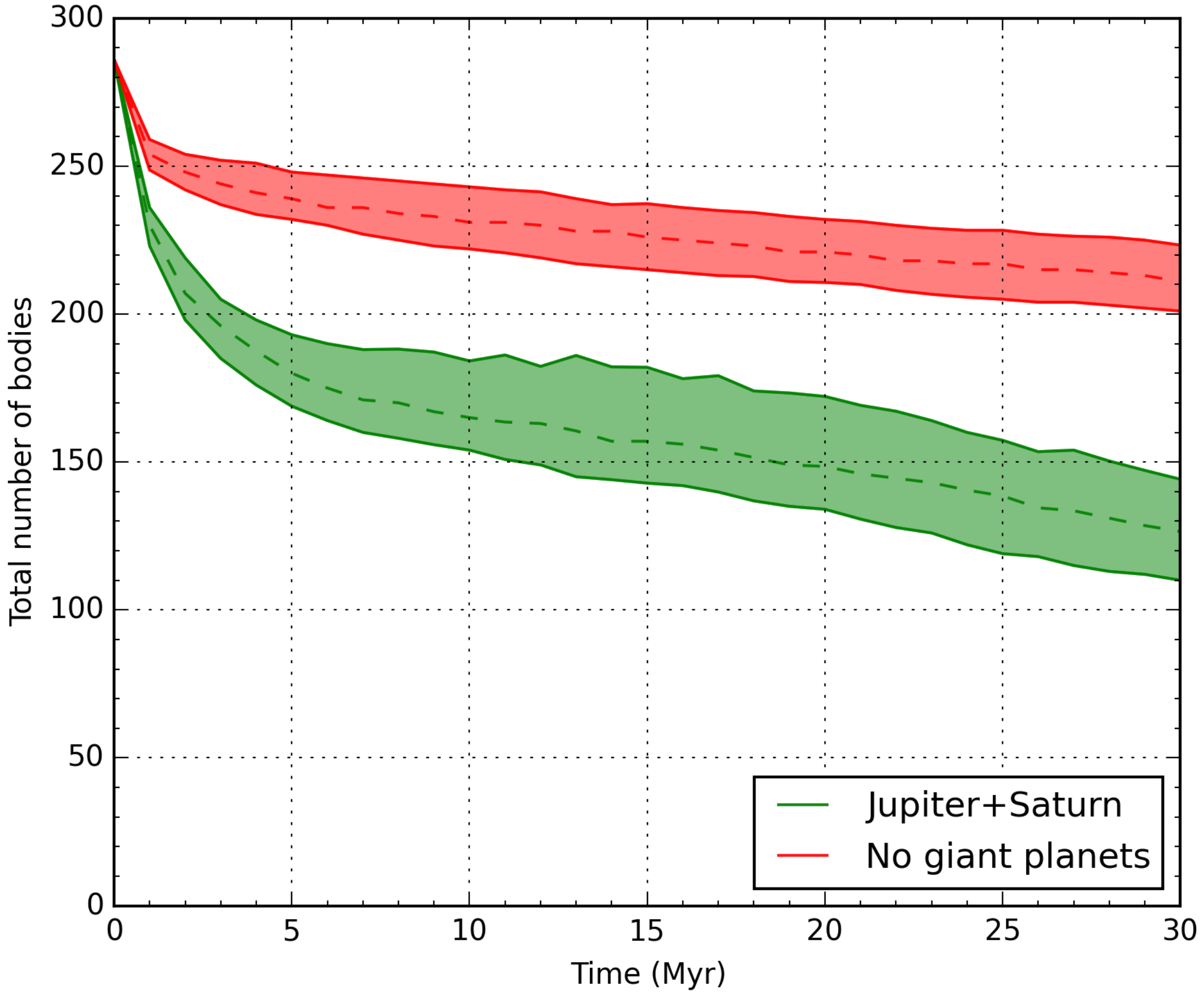

Figure 4.2: Simulation results from Quintana et. al (2016) which consider the two extreme cases for our study: a system with Jupiter and Saturn at their present orbits and a system without giant planets. $1-\sigma$ ranges are shaded for the 140 realizations performed for each system. It is clear that the slopes of both systems slopes begin to flatten around or before five million years. These results give us confidence to limit our computation time to five million years of simulation times for majority of our systems.

Table 4.1: Listed are the varying exterior planet masses and integration times for our simulations. Masses were changed at Jupiter's and Saturn's orbit while maintaining a 3:1 mass ration. All systems were integrated for five myr, except for the extreme case (Jupiter & Saturn) and the intermediate case (150 & $50M_{\oplus}$). These two cases were integrated for 500 myr to ensure trends of mass distribution and orbital evolution of bodies.

System #	Mass at Saturn's orbit ($M_{\oplus}$)	Mass at Jupiter's orbit ($M_{\oplus}$)	Integration time (Myr)
1	95	318	500
2	75	225	5
3	50	150	500
4	30	90	5
5	15	45	5

a system with no exterior giant planets. Their results for numbers of bodies in the system versus simulation time is shown in Figure 4.2. The red is the system with no giant planets, and the green is the system with Jupiter and Saturn. 140 realizations were performed for each system and the number of bodies versus simulation time for all realizations is shown with $1-\sigma$ bounds. From this plot it is clear that a general trend may be determined within the first five myr of simulation time. This motivated us to save computation time and study the intermediate cases with confidence in establishing system trends within the first five myr. Our systems with Jupiter & Saturn and 150 & $50M_{\oplus}$ were integrated for 500 myr to ensure such trends are maintained, and to consider the orbital evolution of the bodies in the system.

4.2 Results

Here we present our results from the 750 simulations for our five different systems, 150 realizations for each system. Each system has an exterior planet of varying mass at Jupiter's

Table 4.2: Listed are the average times at which the system decreases it's number of bodies by 10%, by how many factors more, on average, it took the system to reduce the number of bodies by 10% than the Jupiter & Saturn system, and the ratio of total exterior mass ration of the system compared to the mass of Jupiter+Saturn. We find a steep drop in efficiency to eject 10% of the number of bodies in the system as the mass of the exterior planets decreases.

Exterior masses ($M_\oplus$)	Total exterior mass ratio	Time (Myr)	Time ratio
Saturn & Jupiter	1	0.5 ± 0.1	1
75 & 225	0.73	1.2 ± 0.2	2.4
50 & 150	0.48	1.9 ± 0.3	3.8
30 & 90	0.29	3.7 ± 0.6	7.4
15 & 45	0.15	> 5	> 10

and Saturn's orbit using the same disk with small changes to the longitude of ascending node for one planetesimal. We used a hybrid integrator and the fragmentation code in the N-body integrator, *Mercury*. We discuss the beginning evolution of each of the systems, the final structure of the terrestrial system for the extended runs, and possible mechanisms involved in the giant planet and terrestrial planet interactions.

4.2.1 Evolution of the terrestrial system

The first half-myr of simulation time show the most rapid changes in the system, for all five systems. This is the result of gravity being suddenly turned on in our adopted disk. This time is referred to as the *relaxation time* of the system and it is associated with the time frame for which the system exhibits the largest instabilities. Figure 4.3 shows the number of bodies versus simulation time for our five systems. We may clearly see that the larger the exterior planet masses, the quicker the number of bodies drops in the system. This is the result of larger perturbations to the disk from the more massive exterior giant planets.

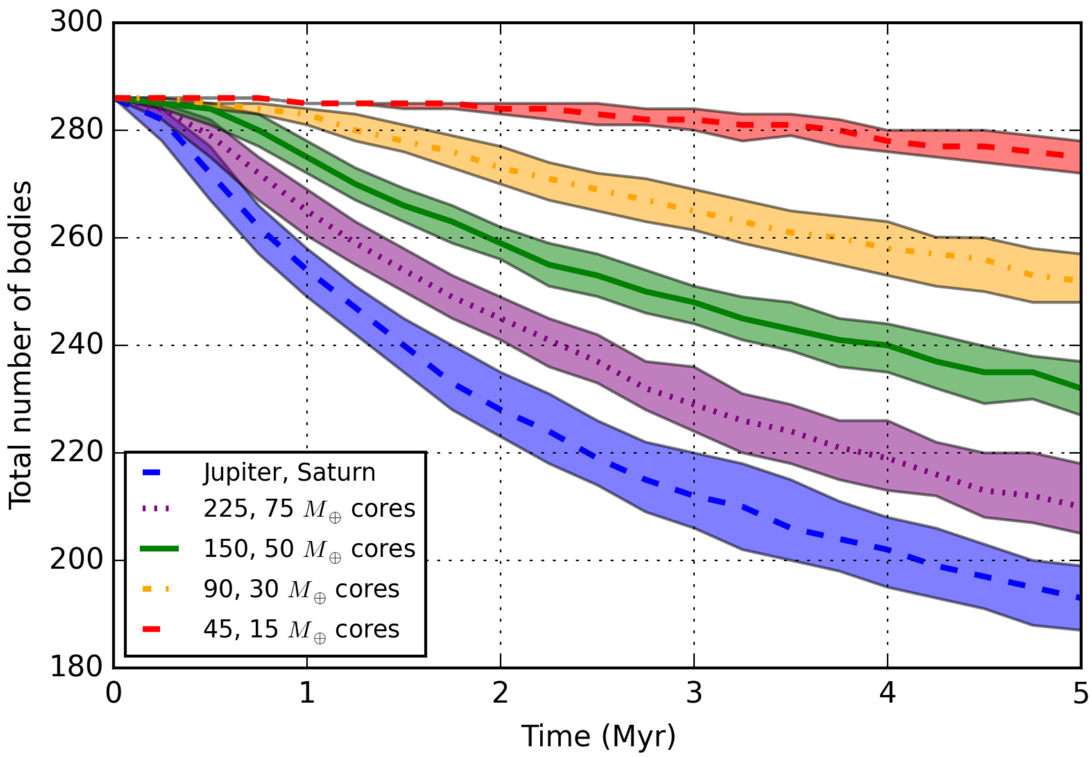

Figure 4.3: A plot of the total number of bodies in the disk (interior to the exterior giant planets) versus simulation time for all 150 realizations of each system. The $1-\sigma$ bounds are shaded and the means are the respective center lines. The number of bodies in the system decreases more quickly as exterior giant planet mass is increased.

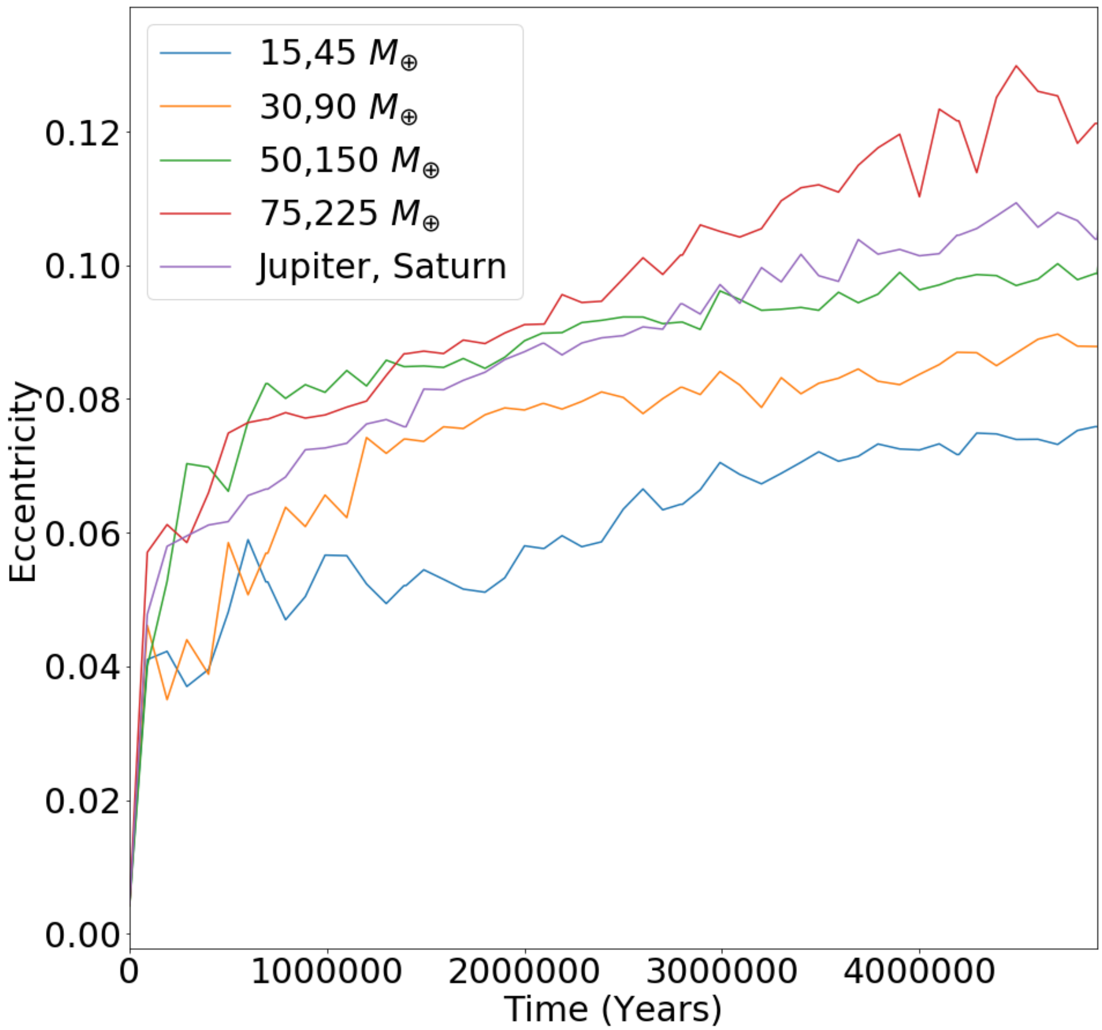

Figure 4.4: A plot showing the median eccentricity evolution of the embryos for each of the five systems. The fastest growth in all of the systems is observed during the *relaxation time* of each system.

Exterior giant planets excite the embryos eccentricities which results in orbit crossings and thus collisions, ejections, and accretion onto the central star (Levison & Agnor (2003)). The median of the eccentricities for the embryos versus time is shown in Figure 4.4. Again there is a correlation between exterior giant planet mass, and rate of eccentricity growth. The fastest growth happens during the *relaxation time* of the system, and the systems with Jupiter & Saturn and with 225 & 75$M_{\oplus}$ cores grow the eccentricities of the embryo's in their system the fastest, while the system with the 15 & 45$M_{\oplus}$ cores grow the eccentricities of the embryo's in their system the slowest. The ability for an embryo to increase its eccentricity over time is important for the terrestrial accretion process as an increase in an embryo's eccentricity allows it to interact with more of the disk (Levison & Agnor (2003)).

Table 4.2 shows the time at which the system decreases its number of bodies by 10% (plus and minus the standard deviation), by how many factors more it took the system to reduce the number of bodies by 10% than the Jupiter & Saturn system, and the ratio of total exterior mass ratio of the system compared to the mass of Jupiter+Saturn. We see that the efficiency to eject 10% of the system's mass quickly decreases as total exterior mass decreases. The second largest system in our study is the system with 75 & 225$M_{\oplus}$ cores at Saturn's and Jupiter's orbit, respectively. All though the total exterior mass of this system is 73% of Jupiter+Saturn, it takes ≈2.5 times longer to eject 10% of the systems bodies. This trend only intensifies as exterior mass decreases, highlighting the importance of perturbations from exterior giant planets on the mass of the system. The smallest system, 45 & 15$M_{\oplus}$, was only able to eject 7% of the bodies in the disk before five million years of simulation time.

For all of our systems, the initial disk mass interior to the giant planets is 4.85$M_{\oplus}$. Figure 4.5 shows the total disk mass of the system versus simulation time, again highlighting the efficiency of ejecting mass for the systems with more massive exterior giant planets. The shaded regions are the $1-\sigma$ bounds, and the center lines show the median for total mass of the system for all 150 realizations. However, the time to eject 10% of the mass for the disk is shorter than the time it takes to eject 10% of the bodies from the disk in most of the systems, suggesting that majority of the bodies ejected from the disk are embryos. Similar to Table 4.2, Table 4.3 lists the mean time (plus and minus the standard deviation) it takes for

Table 4.3: Listed are the average times at which the system decreases it's total disk mass by 10%, by how many factors more, on average, it took the system to reduce the number of bodies by 10% than the Jupiter & Saturn system, and the ratio of total exterior mass ration of the system compared to the mass of Jupiter+Saturn. The smallest system ejected only 3% of it's disk mass before 5 myr of simulation time.

Exterior masses ($M_\oplus$)	Total exterior mass ratio	Time (Myr)	Time ratio
Saturn & Jupiter	1	0.9 ± 0.1	1
75 & 225	0.73	1.6 ± 0.5	1.8
50 & 150	0.48	2.0 ± 0.4	2.2
30 & 90	0.29	3.4 ± 1.5	3.8
15 & 45	0.15	> 5	> 5.6

the system to lose 10% of it's disk mass. Our system with 75 & $225 M_\oplus$ cores took 1.8 times longer to decrease the disk mass by 10% than the system with Jupiter & Saturn. Although this ratio is not as large as the ratio found when considering the decrease in number of bodies, we still see how much more efficient a more massive exterior giant planet is at ejecting mass, than a less massive planet. At 5 myr, the system with 15 & $45 M_\oplus$ cores ejected ≈3% of its disk mass.

Five myr is too early for all of the systems to have reached complete terrestrial planet formation, but it is late enough to see the direction the terrestrial system is headed. Figure 4.6 shows all of the remaining embryos, from all 150 realizations, for each system at ≈5 myr. The figure shows the mass ($M_\oplus$) versus the semi-major axis (AU) of each embryo. From this figure, we can see that the larger the giant planets are, the closer to the host star the embryos are found. From each of these systems, we can also see that the embryo mass is grouped into regimes for each system. For the 45 & $15 M_\oplus$, 90 & $30 M_\oplus$, and 150 & $15 M_\oplus$ systems, we find that there is a grouping of embryos around $\approx 0.1\ M_\oplus$ and a grouping around $\approx 0.2 M_\oplus$. The embryo's have an initial mass of ≈ 0.1 suggesting that for these systems, either the embryos did not gain or lose a significant amount of mass by this

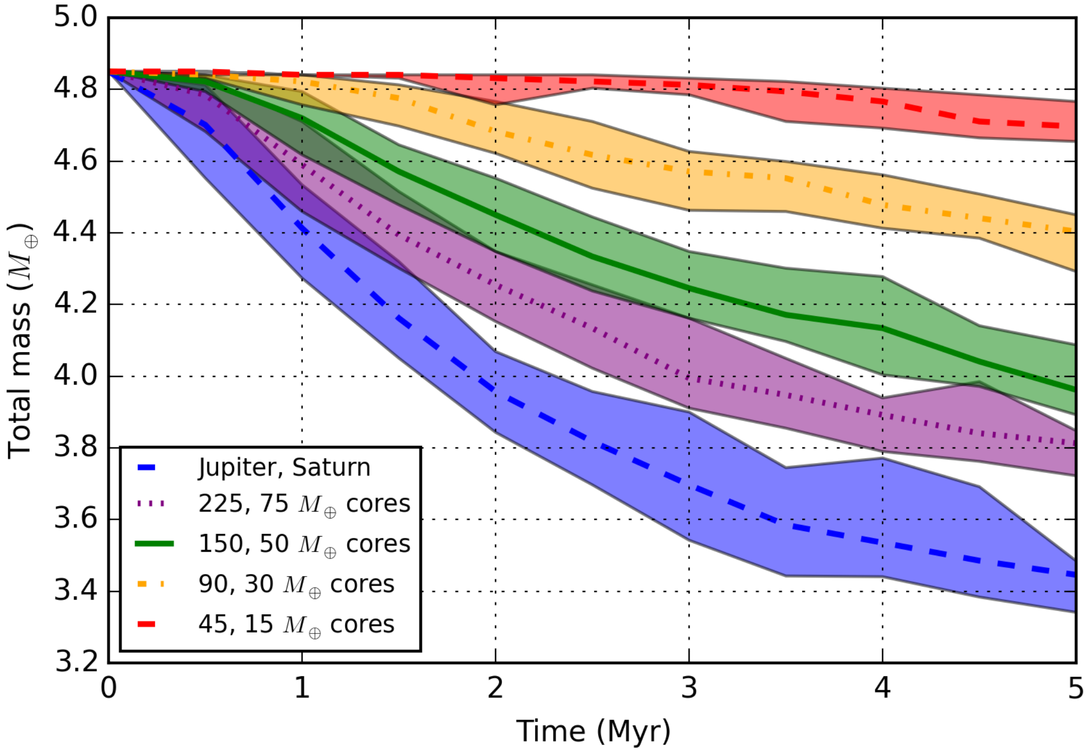

Figure 4.5: A plot of the total mass in the disk (interior to the exterior giant planets) versus simulation time for all 150 realizations of each system. The $1-\sigma$ bounds are shaded and the means are the respective center lines. Disk mass decrease more quickly as exterior giant planet mass is increased as larger exterior planets are more efficient at scattering planetesimals.

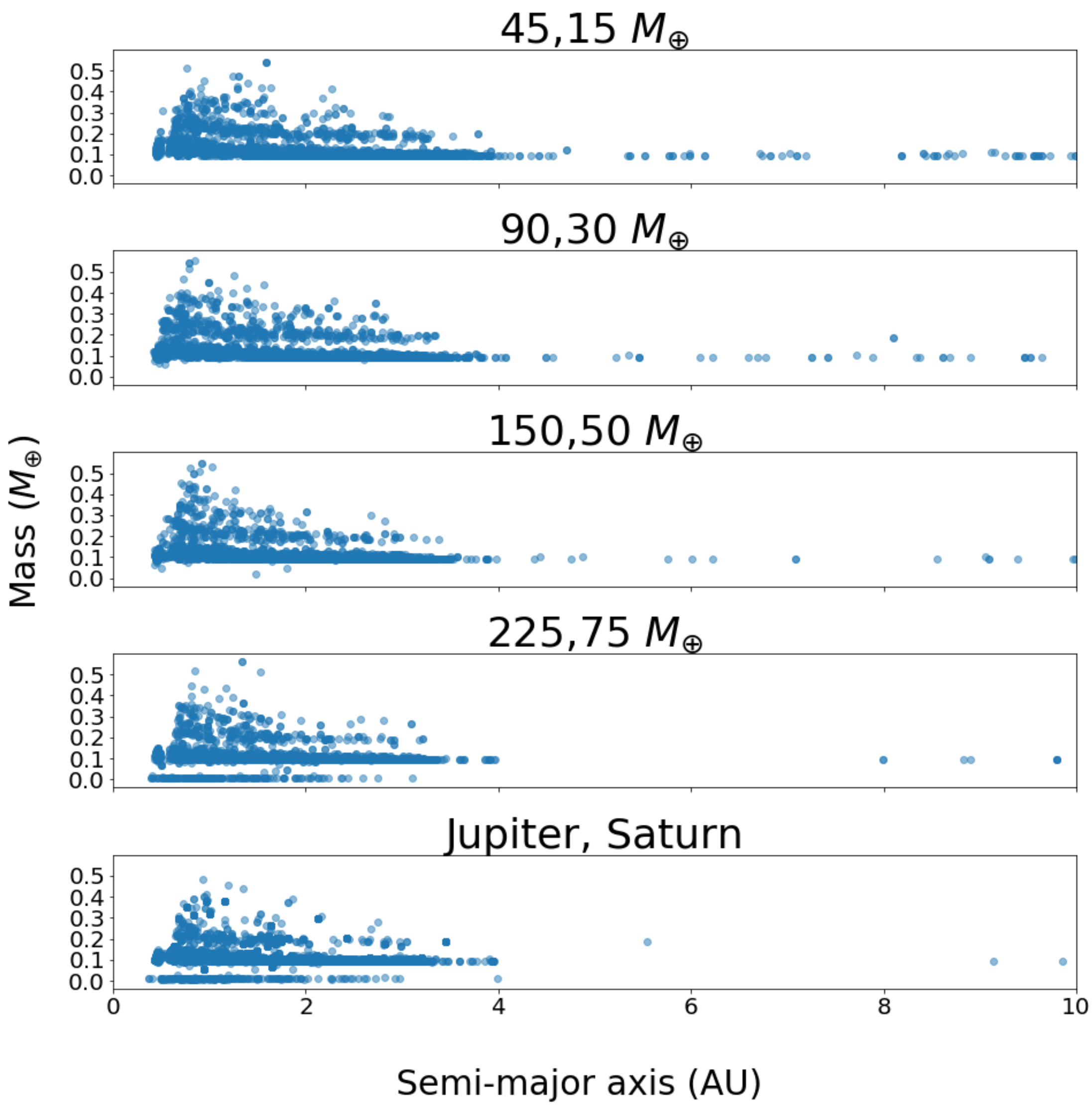

Figure 4.6: A plot of mass ($M_\oplus$) and semi-major axis (AU) for each systems embryos at $\approx$ 5 myr. The masses are found in regimes, different for each system. This suggests that giant planets of different masses promote different collision outcomes.

Table 4.4: Listed are the average masses ($M_\oplus$), semi-major axis (AU), and multiplicities for the embryos in all 150 realizations of each system at ≈ 5 myr.

Exterior masses ($M_\oplus$)	Avg. mass ($M_\oplus$)	Avg. semi-major axis (AU)	Average multiplicity
Saturn & Jupiter	0.12	1.7	16
75 & 225	0.11	1.9	17
50 & 150	0.12	2.0	18
30 & 90	0.13	2.7	19
15 & 45	0.13	2.7	21

time or, they accreted another embryo. The systems with 225 & $75M_\oplus$ cores, and Jupiter & Saturn also have two groupings of mass for their embryos. However, these groupings are around $\geq 0.1M_\oplus$ and $< 0.05M_\oplus$. This suggests that the embryos migrated inwards more quickly, picking up a larger orbital velocity, and collided with one another which resulted in complete fragmentation of some of the embryos, while others survived and accreted the new fragments. Figure 4.7 shows the evolution for an embryo that was demolished by a super-catastrophic collision in one of the 225 & $75M_\oplus$ runs. We see that for the first four myr, this embryo did not lose or gain any mass, but it migrated inwards thus increasing its orbital velocity. As its eccentricity grows it begins to move outwards again until it encounters another body, is completely fragmented due to a high specific impact energy, and then the largest remnant then moves inward again. The average values for the remaining embryos in each of the systems at five myr is summarized in table 4.4.

Again, because of a short simulation time, an analysis of final terrestrial structure is premature. However, the differences between these systems identified at an early time have implications for what the final terrestrial system structure will look like. The next subsection looks at the results for the two systems that were integrated to 500 myr.

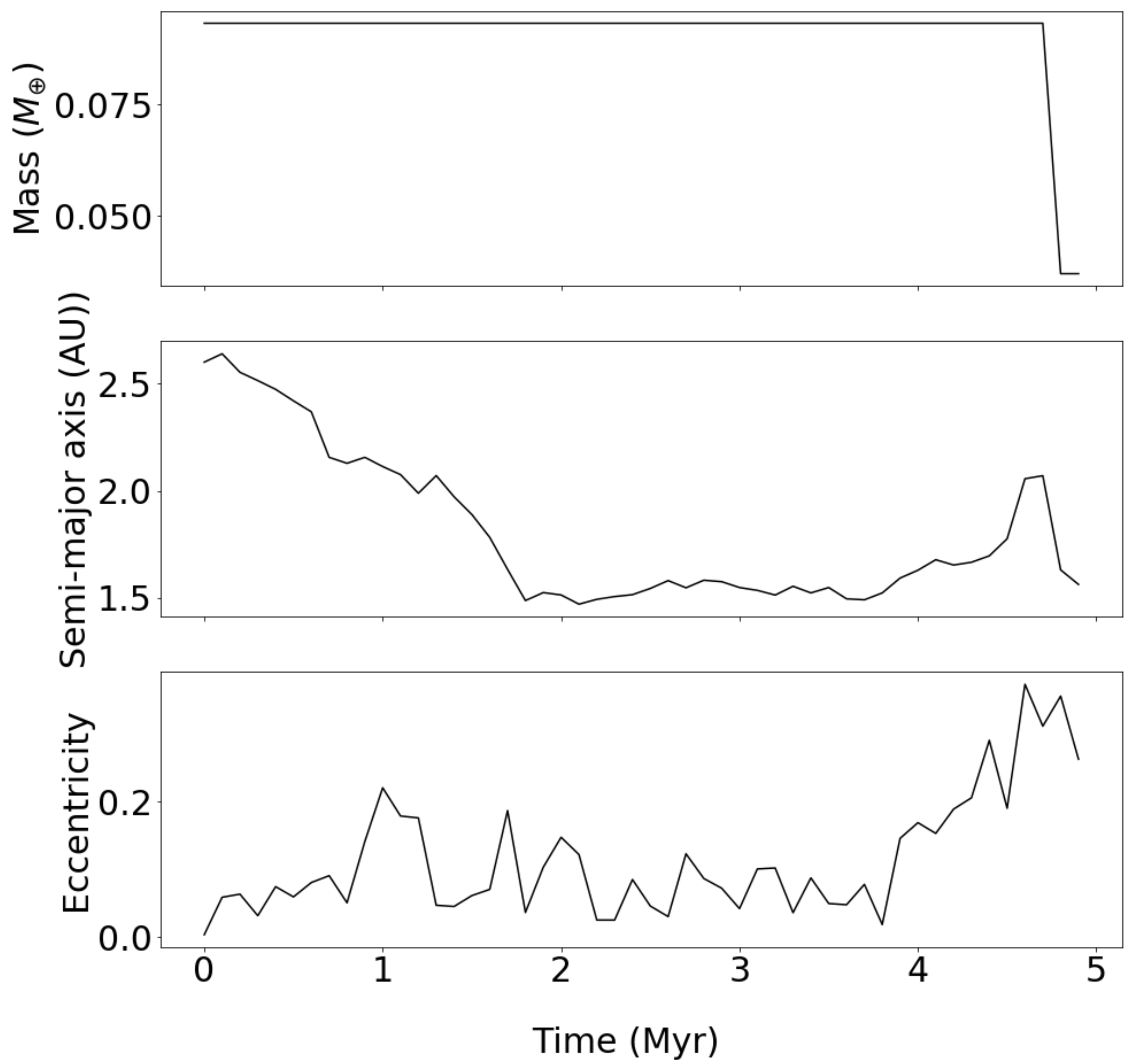

Figure 4.7: A plot of one of the embryos evolution from the 225 & $75 M_\oplus$ system. This embryo was demolished in a super-catastrophic collision. Here we see the evolution of mass, semi-major axis, and eccentricity over five myr for this embryo.

4.2.2 Final terrestrial system characteristics

To understand what the final terrestrial system might look like, we integrated the system with Jupiter & Saturn, and with 150 & $50M_{\oplus}$ cores for 500 myr of simulation time. These runs were extended to ensure that the trends we observe early on in the simulation are maintained with time. Figure 4.8 shows the rate of mass change, versus time on a log scale for all 150 realizations of these two systems. The rate of mass change is given as,

$$\frac{\Delta M}{\Delta t} = \frac{M_f - M_i}{t_f - t_i}, \tag{4.1}$$

where M_f and M_i are the final and initial disk masses (not including the giant planets) in $M_{\oplus}$, and t_f and t_i are the final and initial times in years, respectively. We may clearly see the *relaxation time* for both of these systems as they lose more mass very quickly within the first half myr. This rate begins to drastically slow down and the rates begin to converge and flatten just before 500 myr suggesting that the systems are stabilizing and terrestrial mass loss is nearing completion. The difference in the rates of mass change suggest a different collision history for the two systems. As mentioned before, it is the collision history of embryos which shape the final terrestrial system structure. We may thus conclude that the final terrestrial systems of our two systems, will have different properties.

If we next divide the total mass in the disk by the rate of mass change and take the absolute value, we will get a time scale for the evolution of the system, $\tau_{evolution}$. This expression is given by,

$$\tau_{evolution} = \left| \frac{M_{tot}}{\Delta M/\Delta t} \right|. \tag{4.2}$$

The evolution timescale for all 150 realizations of the Jupiter & Saturn system, and the 150 & $50M_{\oplus}$ system is plotted in figure 4.9 on a log-log scale. It is clear that the evolution timescales associated with the mass loss rate during the *relaxation time* are very short. This is to be expected as this is the time at which the system has the highest rate of mass loss. If such a rate were to be maintained, it would take less than 100 myr for the system to evolve to a state where it has ejected all of its mass. We know that this is not a manifestation of the exterior giants interaction with the disk as much as it is the result of suddenly perturbing the disk by the sudden onset of gravity. However, if we follow the trend we see that the two systems evolution timescales begin to converge as their mass loss rates did. The convergence

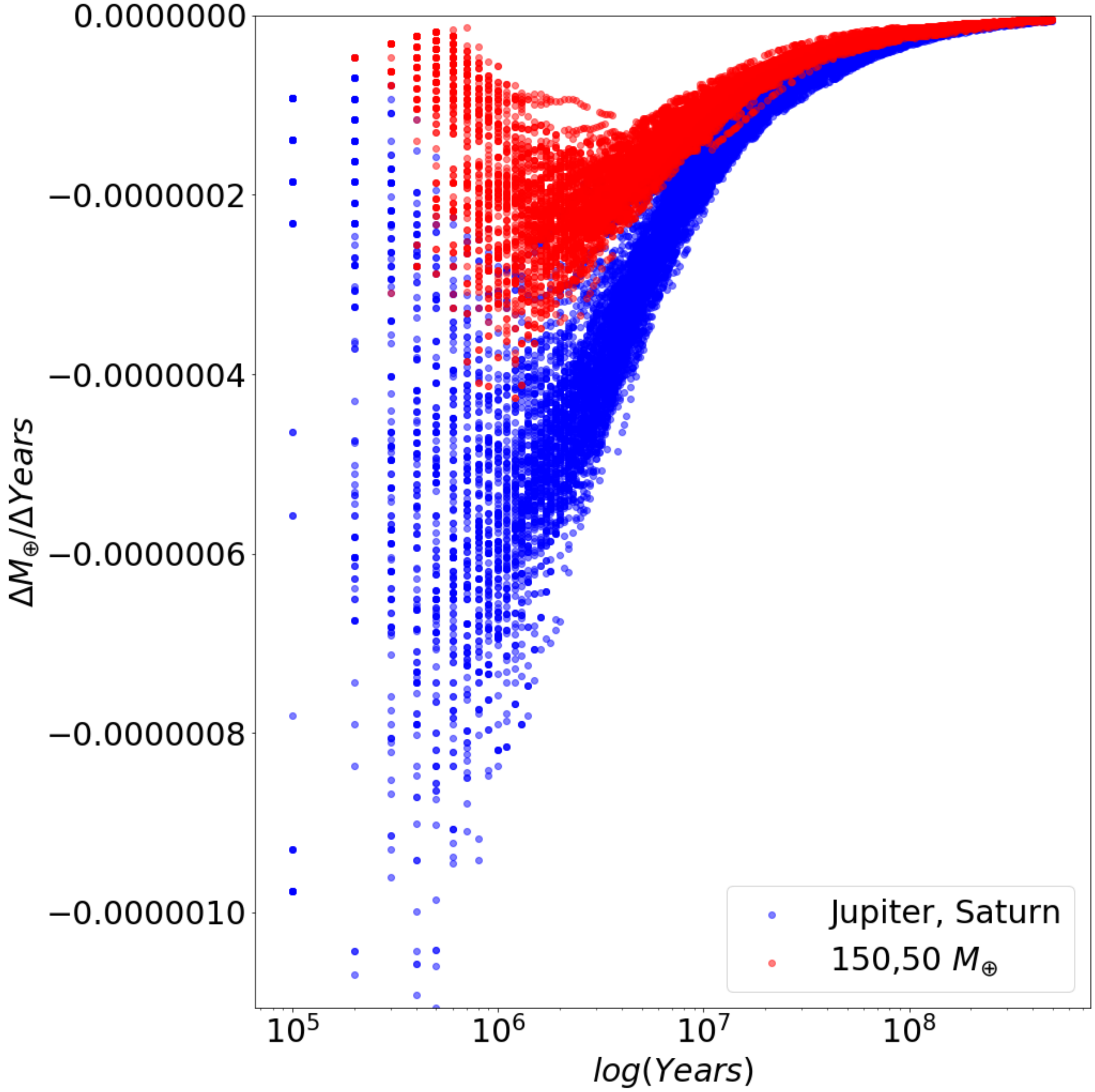

Figure 4.8: This plot shows the rate of mass change (eq. 4.1) versus time for the Jupiter & Saturn system, and the 150 & $50M_\oplus$ cores system. The steep rate of mass change seen within the first half myr is referred to as the *relaxation time* of the system. The two rates begin to converge around ≈ 500 myr suggesting the two systems are stabilizing and nearing terrestrial planet formation completion.

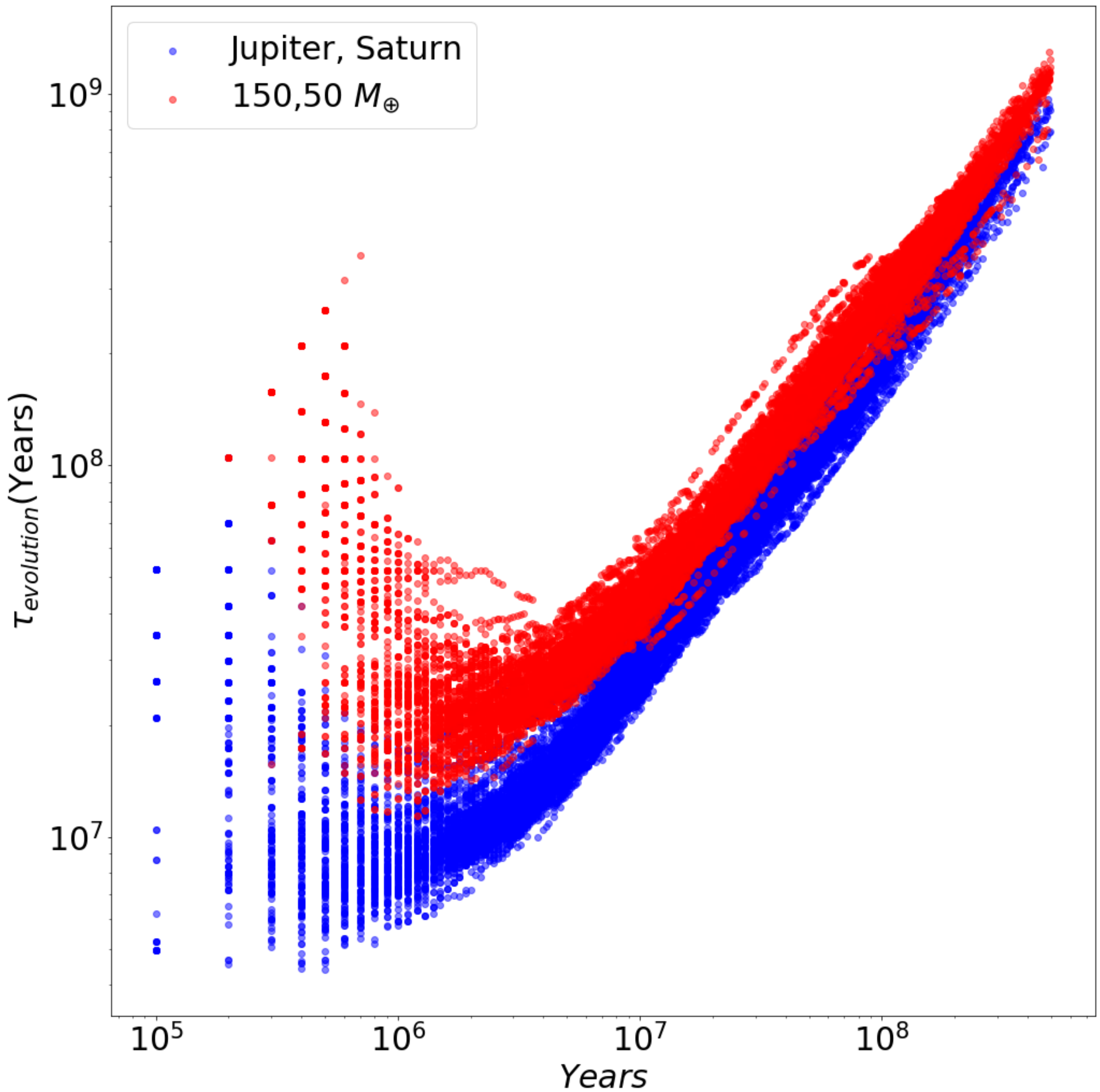

Figure 4.9: The evolution timescale, $\tau_{evolution}$, of the system as defined by eq. 4.2, versus time for the Jupiter & Saturn system, and the 150 & $50M_\oplus$ cores system on a log-log scale. Lower mass loss rates will have a much longer $\tau_{evolution}$.

Table 4.5: Listed are the average masses ($M_{\oplus}$), semi-major axis (AU), and multiplicities for the embryos in all 150 realizations of both of the extended systems at $\approx$ 500 myr.

Exterior masses ($M_{\oplus}$)	Avg. mass ($M_{\oplus}$)	Avg. semi-major axis (AU)	Average multiplicity
50 & 150	0.60	1.49	1
Saturn & Jupiter	0.52	1.3	3

of the two slopes suggests that both of these systems will have similar evolution timescales, all though the system with Jupiter & Saturn will be slightly shorter.

From Figure 4.10 we may see the mass ($M_{\oplus}$) versus semi-major axis (AU) distribution of the embryos in the two extended systems at $\approx$500 myr. What we find is a similar mass and semi-major axis distribution for the two systems, however the Jupiter & Saturn system has more remaining embryos than the 150 & 50$M_{\oplus}$ system. From Figure 4.8 however, we see that no more significant amounts of mass are being ejected from the systems at this time. This implies that the final remaining embryos in the system at this point, will most likely accrete one another until they form stable terrestrial planets. Table 4.5 shows the average masses ($M_{\oplus}$), semi-major axis (AU), and multiplicities for the embryos in all 150 realizations of both of the extended systems at $\approx$ 500 myr. The average remaining disk mass at this time is $\geq$1.56$M_{\oplus}$ for the Jupiter & Saturn system, and $\geq$0.60$M_{\oplus}$ for the 150 & 50$M_{\oplus}$ system. Considering the total mass of the terrestrial planets in our Solar System is $\approx$ 1.98$M_{\oplus}$, this suggest that our adopted disk is a good representation of the Solar System's initial solid disk at the onset of late-stage planet formation.

4.2.3 Program issues and resolutions

Like most programs and updates, *Mercury* with the fragmentation code did not come without bugs. While analyzing the output of the data, we found that *Mercury* began returning erroneous results after an integration was resumed from a dump file. After an integration was resumed from a dump file, all of the bodies were reintroduced in the analysis code called

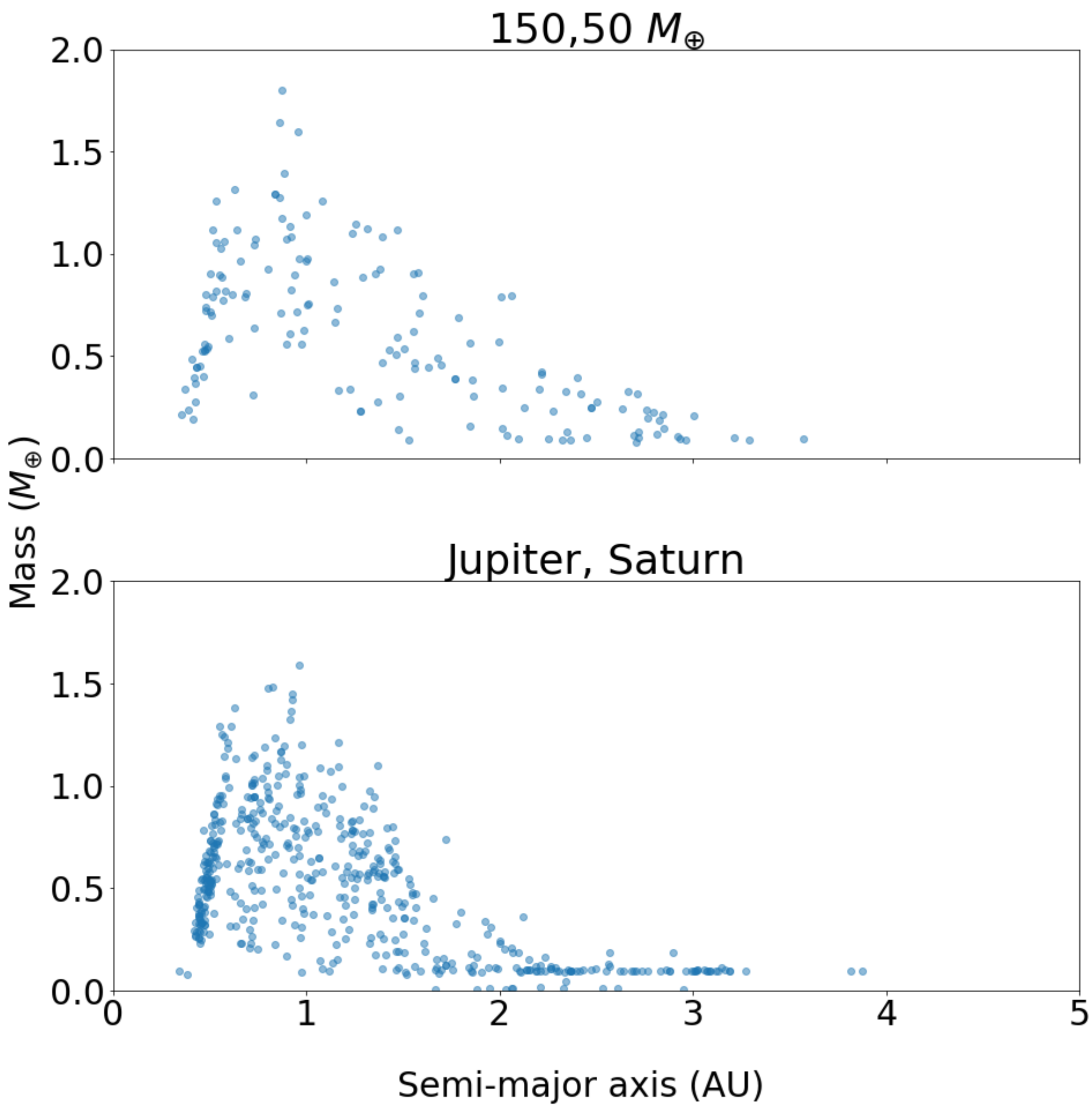

Figure 4.10: A plot of the remaining embryo's mass ($M_\oplus$) and semi-major axis (AU) for the Jupiter & Saturn, and 150 & $50M_\oplus$ systems embryos at $\approx$ 500 myr.

element. As a result, there was data for bodies that had been ejected and two data points with the same time for the surviving bodies. The data was parsed and cleaned. If the bodies were ejected before the integration stopped, the data after the time the body was ejected was ignored. If the bodies survived and had multiple data points at the same time, the higher value data point was ignored. When reviewing the corrupt data, it was clear that the higher value data points were incorrect.

Chapter 5

Exoplanet data and implications

A crucial part of understanding exoplanet science is understanding the current data we have, its limitations, and the expectations and plans we have for future data. Due to the success of previous missions, there has been a big push for future missions to find and observe exoplanets in great detail. Exoplanet data may be collected through a variety of observational methods. These methods include: direct imaging, photometry (also known as the transiting method), radial velocity (RV), and microlensing. Although these detection methods have been widely successful, they each have their own biases and limitations. With our work, we may make prediction about the complete architecture of a planetary system in systems which observations are limited to do so. We may also anticipate results from future missions based on the relationships we have found between giant planets and terrestrial planets.

5.1 Exoplanet detection methods

In this section we will discuss the photometry and radial velocity methods as these are the most common methods for detecting exoplanets, and because each method is sensitive to a different class of planets. RV measurements are sensitive to larger planets, typically found on longer periods, and photometry measurements are sensitive to planets on shorter periods, which typically are smaller terrestrial planets. We will discuss the biases involved with each detection method, and the implications that understanding the relationship between giant planets and terrestrial planets may hold for resolving such biases.

5.1.1 Photometry

A common detection bias of particular importance is the ability of *Kepler* to detect exoplanets with radii $\leq 1.2R_{\oplus}$ around noisy stars (Howell et al. (2016)). If the star's noise is larger than the time scale of transit for an Earth-sized planet, *Kepler* may not detect such a planet. Other planets are more easily detected however, and follow up observation with RV measurements have constrained the mass of many Kepler Objects of Interest (KOI's) (Marcy et al. (2014)). By studying the planet candidates of *Kepler*, we can begin to understand the occurence rates of planets. The most common planets found are small, with radii $< 4R_{\oplus}$. The occurance rate of the planet increases, as the radii decreases to the extent that planets are more common than stars in the Galaxy (Wang et al. (2014)).

Using the Q1-Q16 KOI catalog, and observation from G and K stars, it was determed that just 10% of sun-like stars host planets with radii and orbital periods within 20% that of Earth (Burke et al. (2015)). Another bias is refered to as *false alarms*. This is referred to as periodic signals from intrinsic stellar varability, over-contact binaries, or instrumental noise, being misinterpreted which drastically changes the reliability of planets on long orbital periods Burke et al. (2015).

Although *Kepler* has also found many hot Jupiters, its lack of sensitivity to large orbital periods will not detect giant planets thought to be on longer orbital periods. We may consider *Kepler* systems that are similar to the systems formed in our runs by the presence of giant planets at Saturn's and Jupiter's orbits, and make suggestions about what giant planets could possibly exist in these *Kepler* systems and are not being detected.

5.1.2 Radial Velocity

Giant planets are the easiest to detect via the RV method. Observations from the Keck Observatory showed that 10.5% of $\sim$1000 observed F, G and K-type stars host one or more giant planets with orbital distances of $\approx$0.03-3 AU (Cumming et al. (2008)). Figure 5.1 is a plot from (Howard (2013)) which shows the number of giant planets observed with

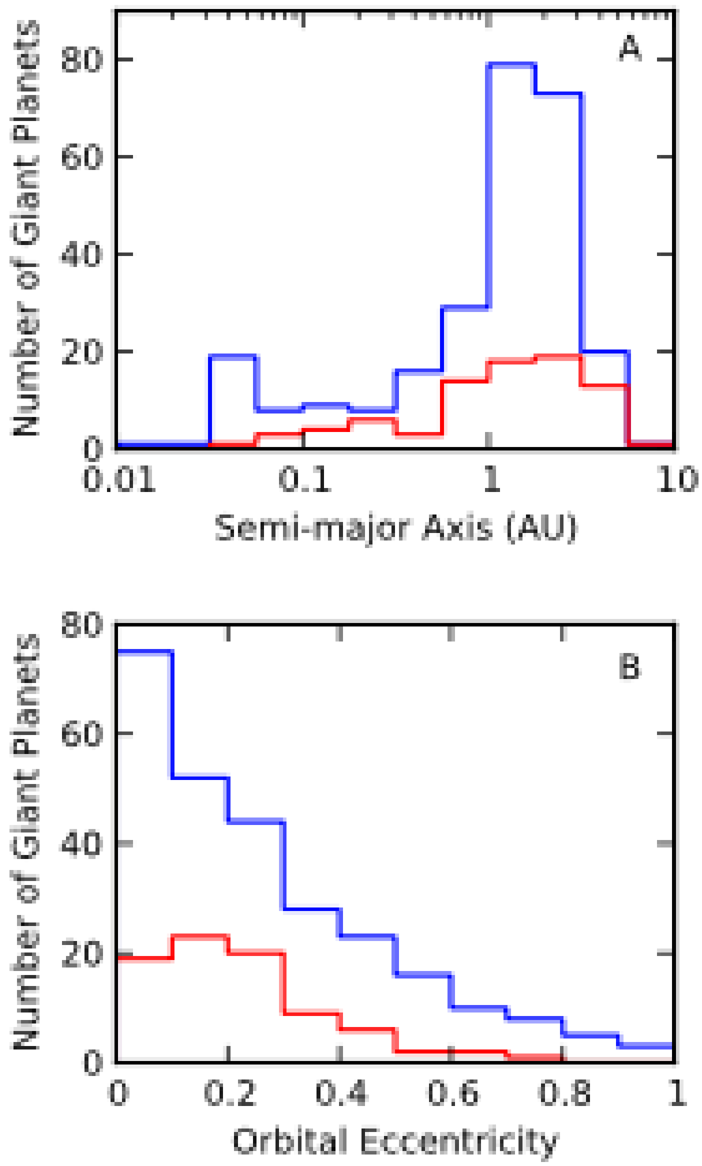

Figure 5.1: Graph A is a histogram of the number of giant planets observed versus semi-major axis. Graph B is a histogram of the number of giant planets observed versus orbital eccentricity of the giant planet. The blue lines represent systems of apparently single planet systems, and the red lines represent systems of multi-planet systems (Howard (2013)).

RV measurements, versus semi-major axis (AU) and orbital eccentricity for systems with multiple planets (red) and systems with apparently single planets (blue). What we find from the histograms is that for both semi-major axis and eccentricity distributions, although we observe higher counts for single planet systems for both, the trends are very similar. Majority of the planets, in both types of systems, have low eccentricities and peak after 1 AU. Because our simulations produced terrestrial planets of fewer multiplicity and closer in to the star, this suggests that this high number of observed single planets could be the result of observation bias. These stars could be harboring multiple planets which are not being observed due to their small size.

5.2 Implications for future work

The transit method has been found to exhibit observational biases for planets on long orbits, and smaller planets around noisy stars. RV methods are not sensitive to small planets and have observed more single-planet giant systems, than multi-planet systems with giant planets. Our studies on the relationship between giant planets and terrestrial planets have shown that giant planets are more likely to form terrestrial planets closer to the host star as the giant planets mass increases. With NASA's *Transiting Exoplanet Survey Satellite* (TESS) expected to launch in June 2018, we may be able to confirm the relationships found between giant planets and terrestrial planets in our simulations, with more detailed observations. TESS will survey stars 30-100 times brighter than the stars *Kepler* sampled. This increase in star brightness will allow TESS to detect exoplanets with smaller radii and the sample of stars will be able to have followup observations done with the *James Webb Space Telescope* (JWST) and other ground and space-based telescopes (Stassun et al. (2017)).

With the detection of smaller exoplanets from TESS and followups from other telescopes, we may get a more complete picture of exoplanet systems and study the relationships between the different planet classes in more detail. Should TESS observe smaller earth planets closer to noisy stars in systems with giant planets, our simulation results and analysis will be further validated.

Chapter 6

Discussion and Conclusions

We have conducted a series of N-body simulations to study the relationship between exterior giant planet mass and terrestrial system architecture using a new collision model. Allowing for fragmentation in N-body simulations leads to a different evolution history which could have important insight into a terrestrial planet's interior structure and moon system. Our emphasis in this study however, is to understand how exterior giant planet masses mold the architecture, with respect to multiplicity, mass and location of the interior terrestrial planet system.

We considered five different systems. Each system has different masses at Saturn's and Jupiter's orbit. The masses maintain a 3:1 mass ratio. We ran 150 realizations of each system, all with the same disk, with the fragmentation code and analyzed the resulting systems at five myr and 500 myr for two of the systems.

We found there does exist a relationship between exterior giant planet mass, and system structure. The higher the masses are at Saturn and Jupiter's orbit, the lower the multiplicity of the terrestrial system, and the larger the planets are. The planets are also found, on average, closer to their host star, than planets with lower massed exterior giant planets. This is due to the exterior giant planets ability to excite the embryo's in the disk. The greater the mass of the exterior giant planets, the more efficient they are at exciting the embryo's eccentricities, and thus scattering bodies out of the system and reaching a stable terrestrial planetary structure more quickly.

We also found that the collision, accretion and fragmentation process differs for the systems. For systems with planets that have a mass ≥ 225 & $75M_{\oplus}$ at Jupiter's and Saturn's orbits respectively, embryos are more likely to result in super-catastrophic collisions. We found that embryos in those systems are more like to experience completely inelastic collisions or cratering. These results give insight to the collision history of terrestrial planets in the presence of exterior giant planets of a given mass. The evolution timescale of the system also depends on the mass of the exterior giant planet mass. The greater the mass of the giant planets, the shorter the evolution timescale will be for the system. This is the result of an exterior giant planets greater ability to perturb the disk and eject mass more efficiently than exterior giant plants of lesser mass.

To date, majority of observational data for exoplanet systems comes from the *Kepler* mission. *Kepler* uses the transit method to detect exoplanets. All though very successful in finding exoplanets, it does not come without its observational biases. Howell et al. (2016) found that photometric noise intrinsic to the star inhibits *Kepler* from finding small terrestrial-size planets with radii $\leq 1.2R\oplus$ around solar type stars. *Kepler* is also not sensitive to planets on long periods, such as the periods of Jupiter and Saturn. RV measurements are good for detecting giant planets, but are not sensitive to smaller planets.

From our simulations, we have found that there exists a relationship between exterior giant planet mass and terrestrial planet formation. The presence of large giant planets would suggest that terrestrial planets are more likely to form closer in to its host star and also that fewer terrestrial planets will be formed. These planets could potentially be missed by *Kepler* and RV measurements due to their small sizer. We hope with the launch of TESS in June 2018, smaller exoplanets will be detected in systems with giant planets with orbits and masses that confirm our results.

Bibliography

Asphaug, E. 2009, Annual Review of Earth and Planetary Sciences, 37, 413. https://doi.org/10.1146/annurev.earth.36.031207.124214

Burke, C. J., Christiansen, J. L., Mullally, F., et al. 2015, The Astrophysical Journal, 809, 8. http://stacks.iop.org/0004-637X/809/i=1/a=8

Chambers, J. 2001, Icarus, 152, 205 . http://www.sciencedirect.com/science/article/pii/S0019103501966394

Chambers, J. E. 2013, Icarus, 224, 43

Cumming, A., Butler, R. P., Marcy, G. W., et al. 2008, Publications of the Astronomical Society of the Pacific, 120, 531. http://stacks.iop.org/1538-3873/120/i=867/a=531

Horner, J., & Jones, B. 2008, International Journal of Astrobiology, 7, 251?261

Howard, A. W. 2013, Science, 340, 572. http://science.sciencemag.org/content/340/6132/572

Howell, S. B., Ciardi, D. R., Giampapa, M. S., et al. 2016, The Astronomical Journal, 151, 43. http://stacks.iop.org/1538-3881/151/i=2/a=43

Leinhardt, Z. M., & Stewart, S. T. 2012, ApJ, 745, 79

Levison, H. F., & Agnor, C. 2003, The Astronomical Journal, 125, 2692. http://stacks.iop.org/1538-3881/125/i=5/a=2692

Marcy, G. W., Isaacson, H., Howard, A. W., et al. 2014, ApJS, 210, 20

Quintana, E. V., Barclay, T., Borucki, W. J., Rowe, J. F., & Chambers, J. E. 2016, ApJ, 821, 126

Rafikov, R. R. 2003, The Astronomical Journal, 125, 942. http://stacks.iop.org/1538-3881/125/i=2/a=942

Righter, K., & O'Brien, D. P. 2011, Proceedings of the National Academy of Sciences, 108, 19165. http://www.pnas.org/content/108/48/19165.abstract

Stassun, K. G., Oelkers, R. J., Pepper, J., et al. 2017, ArXiv e-prints, arXiv:1706.00495

Wang, J., Xie, J.-W., Barclay, T., & Fischer, D. A. 2014, The Astrophysical Journal, 783, 4. http://stacks.iop.org/0004-637X/783/i=1/a=4

Weidenschilling, S. J. 1977, MNRAS, 180, 57

Curriculum Vitae

Anna Corinne Childs E-mail: childs.annacorinne@gmail.com Phone: +1 702/895-0806

Education

MS, Physics, expected December 2017 — University of Nevada, Las Vegas (UNLV)

Advisor: *Jason Steffen, PhD*

BS, Mathematics, 2014 — UNLV

Teaching

Graduate Teaching Assistant of Physics (2017-Present) — UNLV

Graduate Teaching Assistant of Astronomy (2015-2017) — UNLV

Adjunct Instructor of Mathematics (2013-2014) — College of Southern Nevada

Research Experience

Graduate Research Assistant in Exoplanetary Sciences (2015-Present) — UNLV

Research Intern (2016) — NASA Ames

Undergraduate Research Assistant in Physical Chemistry (2011-2013) — UNLV

Conference Presentations

NASA's Bay Area Exoplanet Seminar (2016) — NASA Ames

Awards

Graduate Assistantship (2016-present)	UNLV
Music Scholarship (2009-2014)	UNLV
Millennium Scholarship (2009-2014)	UNLV

Professional references

1. Jason Steffen, PhD, Assistant Professor of Astronomy, UNLV

   E-mail: jason.steffen@unlv.edu

   Phone: +1 702/895-3485

   Website: `http://www.physics.unlv.edu/~jsteffen/`

2. Elisa Quintana, PhD, Research Assistant, NASA Goddard Space Flight Center

   E-mail: elisa.quintana@nasa.gov

   Phone: +1 301/286-0851

   Website: `https://science.gsfc.nasa.gov/sed/bio/elisa.quintana`

3. Scott Lester, Workforce & Coordinator, College of Southern Nevada

   E-mail: scott.lester@csn.edu

   Phone: +1 702/651-4664